Internal quantum efficiencies of AlGaN quantum dots grown by molecular beam epitaxy and emitting in the UVA to UVC ranges

Julien Brault, Samuel Matta, Thi Huong Ngo, Mohamed Al Khalfioui, Pierre Valvin, M Leroux, Benjamin Damilano, Maxim Korytov, Virginie Brandli, Philippe Vennegues, et al.

Internal quantum efficiencies of AlGaN quantum dots grown by molecular beam epitaxy and emitting in the UVA to UVC ranges

J. Brault[1,a)], S. Matta[1,b)], T.-H. Ngo[1,2], M. Al Khalfioui[1], P. Valvin[2],M. Leroux[1], B. Damilano[1], M. Korytov[1], V. Brändli[1], P. Vennéguès[1], J Massies[1], B. Gil[2]

1 : Université Côte d'Azur, CNRS, CRHEA, 06560 Valbonne, France

2 : CNRS-Université Montpellier 2, L2C, UMR 5221, 34095 Montpellier, France

$Al_yGa_{1-y}N$ quantum dots (QDs) have been grown by molecular beam epitaxy on $Al_xGa_{1-x}N$ (0001) using a 2 dimensional – 3 dimensional growth mode transition that leads to the formation of QDs. QDs have been grown for Al compositions y varying between 10% and 40%. The influence the active region design (composition y, QD height and band gap difference (ΔE_g) between the $Al_xGa_{1-x}N$ cladding layer and the $Al_yGa_{1-y}N$ QDs) is discussed based on microscopy, continuous wave photoluminescence (PL) and time-resolved PL (TRPL) measurements. In particular, increasing y leads to a shift of the QD emission towards shorter wavelengths, allowing covering a spectral range in the UV from 332 nm (UVA) to 276 nm (UVC) at room temperature (RT). The low temperature (LT) internal quantum efficiency of the QD ensembles was estimated from TRPL experiments at 8 K, and values between 11 % and 66 % were deduced. The highest IQE-LT are found for the QDs with the higher Al content y. Then, the PL spectrally integrated intensity ratios between RT and LT were measured to estimate the IQE of the samples at RT. The PL ratio is higher for larger ΔE_g, *i.e.* for QDs with y of 0.1 or 0.2, but high PL intensity ratios up to 30% were also measured for QDs with larger y of 0.3 or

[a]Electronic mail: Julien.Brault@crhea.cnrs.fr.
[b] Present address RIBER S.A., 31 rue Casimir Périer, BP 70083, 95873 Bezons cedex, France.

0.4. RT IQE values between 5% and 20% are deduced for $Al_yGa_{1-y}N$ QDs emitting in the 276-308 nm range.

I. INTRODUCTION

$Al_xGa_{1-x}N$ based light emitting diodes (LEDs) can cover the ultra-violet (UV) region over a broad spectral range from 400 nm (UVA) down to 206 nm (UVC) by adjusting the Al composition of the active region.[1] As the replacement of mercury (Hg) lamps by environmentally safe UV sources is targeted in a near future as stated by the Minamata Convention on Mercury,[2] $Al_xGa_{1-x}N$ LEDs are expected to fulfil this goal and have been focusing an increased interest. III-nitride LEDs are mainly grown on sapphire substrates, which are well adapted to UV applications due to its large size availability, low cost and transparency. The research on deep UV LEDs has led to improved performances in the internal and external quantum efficiencies (IQE and EQE, respectively) during the past few years.[3,4,5,6,7,8,9,10] Indeed, IQE as high as 85% at 280 nm,8 EQE above 20% at 275 nm,4 and optical power above 10 mW at 295 nm and 20 mA9 were reported recently. But there is still room for improvement, in particular for monolithic growth approaches of high Al content $Al_xGa_{1-x}N$ heterostructures grown on sapphire which are typically characterized by high threading dislocation densities (TDDs) in the $10^9 – 10^{10} cm^{-2}$ range.[11] Such high TDDs lead to low internal quantum efficiencies (IQE) in $Al_yGa_{1-y}N/Al_xGa_{1-x}N$ quantum well (QW) active regions,[12,13] and to UV LEDs with limited performances. This is often observed for molecular beam epitaxy (MBE) fabrication processes from which UV LED performances still lag behind those of metalorganic vapor phase epitaxy (MOVPE) because of the difficulty to reach TDDs below 10^9 cm^{-2}. Yet, strategies to improve the radiative efficiency of $Al_yGa_{1-y}N$ / $Al_xGa_{1-x}N$ heterostructures have recently been proposed relying on the creation of in-plane confining regions based either on quantum engineering at the monolayer (ML) level,[14,15,16] or using specific growth conditions to favour

band structure potential fluctuations[17] and compositional modulation using misoriented surfaces.[18] In particular, $Al_yGa_{1-y}N$ based active regions grown by MBE under Ga rich conditions were introduced to promote potential fluctuations and improve the EQE of UV LEDs.[19] Another possibility is the formation of $Al_yGa_{1-y}N$ quantum dots (QDs), which is well mastered using MBE.[20,21,22] Such engineering of the active region may inhibit the transfer towards non radiative centers of excitons leading to a weak temperature dependence of the photoluminescence emission and to higher IQE.[23,24] The use of a compressively strained $Al_yGa_{1-y}N$ layer on top of AlN has been shown to efficiently lead to the formation of QDs, and to get an emission in the deep UV, *i.e.* down to 235 nm.[25] Following a similar path and using $Al_xGa_{1-x}N$ surfaces in order to avoid the difficulty of AlN *n*- and *p*-type doping,[26] we have shown the possibility to fabricate $Al_yGa_{1-y}N$ QDs with a nominal concentration y of 10% on $Al_{0.5}Ga_{0.5}N$ (0001), emitting from 340 down to 314 nm at room temperature, by varying the $Al_yGa_{1-y}N$ amount deposited to grow the QDs.[27] Furthermore, LED structures based on QDs as active regions were recently reported using different designs, *i.e.* tunnel injection,[28] polar[20] or semi-polar orientations,[29] varying the QD heights[30] and compositions,[31] and have shown their potential for UV sources covering a broad wavelength range.

In this work, several parameters have been investigated to design different $Al_yGa_{1-y}N$ QDs / $Al_xGa_{1-x}N$ (0001) active regions by changing x and/or y compositions: the effect of the lattice-mismatch, of the band gap difference between the $Al_xGa_{1-x}N$ cladding layer and the $Al_yGa_{1-y}N$ QDs, of the QD Al composition y and/or of the $Al_yGa_{1-y}N$ deposited amount. In particular, it is found that for QDs grown on $Al_{0.7}Ga_{0.3}N$, the emission can be tuned from 332 nm down to 276 nm by increasing the Al composition y from 10% to 40%. Also, the IQE has been estimated for the different QD active regions by combining temperature dependent photoluminescence (PL) and time resolved photoluminescence measurements (TRPL) and temperature dependent photoluminescence (PL) measurements, indicating a strong dependence

with the Al composition of both the QDs and the cladding layer. IQE values varying between 5% and 20% were determined at room temperature for $Al_yGa_{1-y}N$ QDs emitting in a wavelength range between 276 and 308 nm.

II. EXPERIMENTAL METHOD

A. SAMPLE FABRICATION

The samples were grown on (0001) sapphire substrates by molecular beam epitaxy (MBE) in a RIBER 32 reactor using solid sources for the III-elements, and ammonia (NH_3) as nitrogen precursor except for the fabrication of the QD layers which were grown using a RIBER RF nitrogen (N_2) plasma source.[23] Indeed, the growth of compressively strained (Al,Ga)N layers with an N_2 source leads to a 2 dimensional (D) - 3D growth mode transition and the formation of 3D islands during the deposition,[23] contrary to the use of NH_3 as nitrogen source for which a 2D growth mode is obtained whatever the deposited thickness.[32] However, the growth of thick (Al,Ga)N templates is performed by using NH_3, because the growth conditions of 2D layers are easier to master.[33] The structure layout consists of a low-temperature GaN buffer layer of 30 nm, followed by the deposition of a 100-150 nm thick AlN layer at 950°C, and a 800-1000 nm thick $Al_xGa_{1-x}N$ layer with an Al composition of 50% or 70% grown at 850 or 870°C, respectively (figure 1).

Next, the QDs were formed by depositing $Al_yGa_{1-y}N$ with an Al nominal concentration y of 0.1, 0.2, 0.3 or 0.4. The QD composition was determined by adjusting the AlN over GaN growth rate ratio, which is equal to the Al over Ga concentration ratio in the QDs. The QDs were formed on $Al_{0.5}Ga_{0.5}N$ or $Al_{0.7}Ga_{0.3}N$ surfaces following a 2D - 3D growth mode transition. A growth rate of 0.2± 0.05 ML/s and a growth temperature of 720°C ± 20°C were used. After the deposition of the $Al_yGa_{1-y}N$ layer, an annealing step under vacuum of the QD layer was performed for 6 minutes with a progressive temperature increase up to 820°C ± 10°C

as described in ref. 23. The QD layer was then capped with a 30 nm $Al_xGa_{1-x}N$ barrier having the same composition as the template layer, and was followed by the growth of a surface uncapped QD layer identical to the buried one.

In order to investigate the influence of the active region design on the structural and optical properties of $Al_yGa_{1-y}N$ QDs, a series of samples (labelled from A to G) have been fabricated (table 1). The QD structures were grown by depositing $Al_yGa_{1-y}N$ amounts with thicknesses (corresponding to a 2D layer growth) between 6 and 10 monolayers (MLs), with 1 ML being half the c lattice parameter, *i.e.* between 0.253 and 0.258 nm considering a variation of the lattice parameter following a Vegard's law between GaN and AlN. Samples A to C consist of $Al_{0.1}Ga_{0.9}N$ QDs: deposited amounts equivalent to 10 MLs were used in samples A and C, whereas for sample B only 7 MLs were deposited. The QDs were inserted in an $Al_xGa_{1-x}N$ cladding layer with x equals to 0.5 for samples A and B and with x equals to 0.7 for sample C. For the other samples, the active region consists of $Al_yGa_{1-y}N$ QDs in an $Al_{0.7}Ga_{0.7}N$ cladding layer with y varying from 10% to 40% from samples D to G, respectively. An $Al_yGa_{1-y}N$ deposited thickness of 10 MLs was used for sample D, of 8 MLs for sample F, and of 6 MLs for samples E and G.

B. CHARACTERIZATION METHODS

The heterostructures were characterized by X-ray diffraction (XRD) using a four-circle diffractometer to study the crystalline quality of the $Al_xGa_{1-x}N$ layers by performing ω-scans of the (0002) symmetric reflection and the (30-32) skew asymmetric reflection. The morphology of the uncapped QD layer was investigated by *ex-situ* atomic force microscopy (AFM) operating in tapping mode. In addition, cross-sectional transmission electron microscopy (TEM) measurements were performed. The TEM specimens were prepared by mechanical polishing followed by ion milling. High-angle annular dark-field imaging in scanning

transmission electron microscopy mode (STEM-HAADF) was performed using a Titan 80-300 electron microscope (300 kV), and the images have been taken along the [11-20] zone axis.

Regarding the optical characteristics, continuous wave photoluminescence (PL) measurements were carried out at room temperature (RT) and low temperature (LT), *i.e.* at 300 K and 8K, respectively, in a closed cycle He cryostat and using a frequency-doubled Ar laser at 244 nm (5.08 eV). The excitation power was set to 30 mW, which gives an excitation power density of 470 W/cm^2). In particular, the ratio of the spectrally integrated PL intensity of the QD emission was determined between LT and RT. Also, LT time-resolved PL (TRPL) measurements were performed using a mode-locked frequency-tripled titanium–sapphire laser with a wavelength of 260 nm (4.77 eV). The laser excitation power was about 200µW, with a laser spot size of 100µm, giving an average excitation power density of about 2-3 W/cm^2. The timescale between two successive laser pulses (with a value of 12 or 250 ns, depending on the sample) was selected to be longer than the decay times of the samples (ranging between 800 kHz and 82 MHz), *i.e.* with repetition rates ensuring a complete decay of the PL and adapted to the decay times of each sample. As detailed in the following section, the combination of TRPL and RT-LT PL measurements was used to determine and compare the IQE of the different $Al_yGa_{1-y}N$ QD active regions.

III. RESULTS AND DISCUSSION

1. Structural properties

Broad XRD peaks with full width at half maximum (FWHM) in the range of 0.4-0.5° for the (002) reflection and in the range of 0.7-1° for the (302) reflection have been measured on the sample series. Based on our previous results obtained on $Al_{0.5}Ga_{0.5}N$ and AlN layers grown on sapphire,[34,35] the TDDs in the heterostructures were estimated from these measurements (and assessed by TEM measurements performed on reference samples) based on

the model used in ref. 35: screw type dislocation densities are in the 4–7x10^{9} cm^{-2} range (from the (002) peak FWHM) and mixed plus edge dislocation densities in the 3.5–7x10^{10} cm^{-2} range (from the (302) peak FWHM). Therefore, we estimate an average TDD value of 6(± 2)x10^{10} cm^{-2} in the samples investigated.

In order to study the influence of the active region design on the structural and optical properties of the QDs, the samples present differences in either: i) the QD composition, ii) the band gap energy difference (ΔE_g) between the QD and the cladding layer, determined from the Al composition difference between the $Al_yGa_{1-y}N$ QD and the $Al_xGa_{1-x}N$ cladding layer and referred as $\Delta x\text{-}y = x - y$ in the following , or iii) the $Al_yGa_{1-y}N$ deposited amount (see figure 1 and table 1).

Besides giving qualitative information about the QD formation, the RHEED Bragg spot intensity variation during growth was also investigated to determine the deposited $Al_yGa_{1-y}N$ critical thickness for the 2D – 3D growth mode transition ($h_{2D\text{-}3D}$).[36] In particular, the influence of the lattice-mismatch ε (with $\varepsilon = \Delta a/a_{AlxGa1-xN}$ and $\Delta a = a_{AlyGa1-yN} - a_{AlxGa1-xN}$) was studied in the case of the growth of $Al_yGa_{1-y}N$ layers on $Al_{0.7}Ga_{0.3}N$ (0001) while changing the QD composition: it was found that the critical thickness $h_{2D\text{-}3D}$ increases from (3 ± 0.5) MLs to (4 ± 0.5) MLs while going from $Al_{0.1}Ga_{0.9}N$ to $Al_{0.4}Ga_{0.6}N$ QDs. The main reason for this increase is attributed to the in-plane lattice parameter difference between the deposited $Al_yGa_{1-y}N$ and the $Al_{0.7}Ga_{0.3}N$ layer, since increasing y from 0.1 to 0.4 induces a decrease of ε from 1.5% for $Al_{0.1}Ga_{0.9}N$ down to 0.75% for $Al_{0.4}Ga_{0.6}N$. Indeed, the value of ε has a fundamental influence on the QD formation mechanisms through the energetic balance between elastic and surface energy variation as the layer morphology undergoes the 2D – 3D growth transition.[37,38] As expected, the QD average dimensions are also modified by the different sample design and growth conditions, as summarized in table 1: the average QD heights are found to vary between 1.5 and 2.6 nm and the densities between 1.5 and 5.4x10^{11} cm^{-2}. Regarding the QD mean

diameters, a weak variation was observed between 8 and 10 nm. Typical AFM images of the whole sample series are presented in figure 2. In the case of the four $Al_yGa_{1-y}N$ QD layers grown on $Al_{0.7}Ga_{0.3}N$ (0001) (corresponding to samples C, D, E, F), STEM characterization was also done and images are presented in figure 3. Regarding the QD density, no specific trend among the samples was observed. In fact, high QD densities (above 10^{11} cm^{-2}) are systematically observed in the case of $Al_yGa_{1-y}N$ QDs compared to GaN QDs[23] and this characteristic is attributed to the lower surface mobility of Al adatoms compared to Ga ones. Regarding the QD average height, it was estimated from the cross-section HAADF-STEM images (figure 3) and from previously characterized samples of $Al_{0.1}Ga_{0.9}N$ QDs grown on $Al_{0.5}Ga_{0.5}N$,[22] as in the case of samples A and B. The images show $Al_yGa_{1-y}N$ QDs for y values of 0.1, 0.2, 0.3 and 0.4 in figures (a) to (d) (corresponding to samples C, D, E and F, respectively). The $Al_yGa_{1-y}N$ layer, which is composed of heavier material than the $Al_{0.7}Ga_{0.3}N$ matrix, has a brighter contrast. A modulation in the $Al_yGa_{1-y}N$ layer thickness can be observed on the different images and the maxima are attributed to the presence of QDs. In the cases of $Al_{0.3}Ga_{0.7}N$ and $Al_{0.4}Ga_{0.6}N$ QDs, the difficulty to define the QD shape is seen as a consequence of the reduced values of ε lower ε are leading to an increase of the wetting layer (WL) thickness as observed in the case of GaN QDs grown on $Al_{0.5}Ga_{0.5}N$[39] compared to GaN QDs grown on AlN.[36] This feature, combined with a larger critical thickness $h_{2D\text{-}3D}$ when ε decreases, then leads to lower aspect ratio values of the QD heights over the WL thickness as the QD Al composition increases. As a general trend, it is found that the QD height increases with larger $Al_yGa_{1-y}N$ deposited amounts (table 1), as already reported for the cases of $Al_yGa_{1-y}N$ (y = 0.1) QDs grown on AlN[21] and of $Al_yGa_{1-y}N$ (y= 0.1) QDs grown on $Al_{0.5}Ga_{0.5}N$.[22]

2. Optical properties

In order to investigate the efficiency of $Al_yGa_{1-y}N$ QDs grown on $Al_xGa_{1-x}N$ as emitters in the UV range, PL and TRPL measurements have been performed, with the objective to give

an estimation of the QD IQE. In the section below, the main results obtained by PL are presented, followed by the TRPL results in the following section. Finally, the analysis of these measurements to estimate the $Al_yGa_{1-y}N$ QD IQE is done in a third section.

2.1. Continuous wave photoluminescence

The optical properties of the samples were investigated by PL as presented in figures 4 and 5. The normalized PL spectra of the complete sample series measured at RT are presented in figure 4: they show the possibility to tune the emission of $Al_yGa_{1-y}N$ QDs from the UVA down to the UVC, with a maximum peak intensity decreasing from around 332 nm (for samples A and C), down to 276 nm (for sample G) by increasing the QD Al composition y from 10% to 40%. A comparison of the RT PL intensity between the samples has shown a decrease of the intensity by a factor of 3 to 4 from 332 nm to 301 nm. A decrease by a factor of 4 to 5 was also observed in the PL intensity from 301 nm to 276 nm. The QD peak emission wavelengths (and corresponding energies) at maximum intensity for the complete sample series are summarized in table 1. Precisely, $Al_yGa_{1-y}N$ QDs with y equals to 0.1 enable to reach the short wavelength region in the UVA and the long wavelength region in the UVB, between 314 and 332 nm, whereas GaN QD emission was previously shown to be limited to the UVA with shortest wavelengths around 360-370 nm.[29] Further increasing the QD Al concentration y to 0.2-0.3 leads to an emission at shorter wavelengths between 297 and 308 nm. Finally, in the case of a QD composition y of 0.4, the UVC region is reached at 276 nm. Benefiting from the quantum confinement effect, a reduction of the deposited amount leads to a blue shift of the wavelength emission into the deeper UV range, as observed for samples B vs. A and G vs. F (table 1). These measurements allow determining that the main parameters influencing the $Al_yGa_{1-y}N$ QD properties in terms of wavelength spectral range are the Al QD composition y, and the $Al_yGa_{1-y}N$ deposited amount. In fact, the PL properties of QDs can be deduced from the QD height as a first approximation since the QD base to height ratio is around 4 (see table 1) : in this case,

due to the high effective mass in nitrides, lateral confinement effects are minimized compared to confinement effects along the growth direction, in agreement with the original work on GaN QDs grown on AlN reported by T. Bretagnon et al.[40]

PL measurements at LT and RT were performed on the whole sample series and the results are presented in figure 5. For all the samples, two broad peaks are observed at LT. The peak at higher energy, and with the lowest intensity, corresponds to the emission from the cladding layer, and is found at around 4.6 (± 0.05) eV for $Al_{0.5}Ga_{0.5}N$ and 4.9 (± 0.1) eV for $Al_{0.7}Ga_{0.3}N$ in agreement with the energy variation trend of localized band edge excitons reported for $Al_xGa_{1-x}N$ alloys up to x equals 70%.[41] Regarding the second peak, which is the most intense one, it originates from the exciton radiative recombination in the $Al_yGa_{1-y}N$ QDs. As shown in the figures, only a weak decrease of the PL intensity is found for the QD PL peak from LT to RT, whereas the PL signal of the cladding layer vanishes completely. These results confirm the strong carrier confinement in the $Al_yGa_{1-y}N$ QDs (with y ranging from 0.1 to 0.4) favouring radiative carrier recombination mechanisms despite the very high TDDs. The spectrally integrated PL intensity ratio (R_{PL}) of the QD emission peak between RT and LT has been determined and is given in table 2. Although the TDD in the samples is above 10^{10} cm^{-2}, R_{PL} values from 0.1 up to 0.3 have been measured in the whole wavelength range. In the case of MBE grown QWs, R_{PL} ratios of 0.01 or below have been reported.[30,23] Noteworthy, values of R_{PL} are observed to vary for QDs emitting in a similar energy range (*i.e.* samples A vs. C, B vs. D and E vs. F) within a factor up to 3. A comparison of the different sample designs indicates that:

i) R_{PL} tend to increase with an increase in Δx-y from 0.4 to 0.5-0.6 (*i.e.* with an increase of the band gap energy difference between the QD and the cladding layer) in the case of $Al_yGa_{1-y}N$ QDs with y = 0.1 – 0.2. Although increasing Δx-y leads to an increase of the polarization-induced electric field, *i.e.* to lower

radiative transition rates, this effect is limited in the present case since the heights of the QDs are small (< 3 nm), similarly to the case of GaN QDs discussed in ref. 29;

ii) Highest R_{PL} ratios are found at higher energies in the 4 – 4.5 eV range, *i.e.* for QD Al compositions y between 0.2 and 0.4 ;

iii) The QD height, determined by the $Al_yGa_{1-y}N$ deposited amount, has no significant impact on the R_{PL} value for y ranging between 0.1 and 0.3 ;

iv) R_{PL} ratios do not show a dependence on the QD density in the investigated range of $1.5x10^{11}$- $5.4x10^{11}$ cm^{-2};

v) In the case of QDs with higher Al compositions, *i.e.* for y = 0.3 – 0.4, a specific behaviour is observed with: 1) a strong variation of the R_{PL} ratio as a function of the $Al_yGa_{1-y}N$ deposited amount, and 2) a value of R_{PL} up to 0.3 although the band gap energy difference between the QD and the cladding layer is relatively low, *i.e.* Δx-y is equal to 0.3 or 0.4.

Noteworthy, the QD densities are found within a magnitude of 3 to 10 higher than the average TDDs in our samples. Consequently, even if dislocations could potentially penetrate into the QDs, the majority of QDs would not be affected by dislocations: this is the main reason why the QD density does not play a role on the PL intensity ratios in our experiments. The situation could eventually be different in the case of QD densities similar or lower than the TDDs: in such a case, the penetration of dislocations into the QDs could significantly reduce the PL efficiency. Indeed, it was shown in TEM studies that GaN QDs can nucleate next to threading edge dislocations,[42] and we have also observed such features in low GaN QD density samples. However, the penetration of a dislocation into a QD is rarely observed since they are nucleating in the vicinity of a dislocation. Indeed, while looking at the PL results in the case of

GaN QDs on $Al_xGa_{1-x}N$ for which densities in the 10^{10} cm^{-2} range have been obtained, we have observed that the integrated PL ratio R_{PL} remains above 0.1 and can even reach 0.6.[23]

2.2. Time-Resolved Photoluminescence

To further investigate the QD optical characteristics and to estimate the internal quantum efficiency (IQE), we have also performed TRPL measurements at LT, as presented in figure 6. For all the samples, it is found that the PL transients exhibit a two-exponential decay behaviour, which is attributed to the presence of non-radiative recombination channels unsaturated in the photo-injection conditions.[43] As described in refs. 22 and 23, the time dependence can be fitted by considering fast (τ_{fast}) and long (τ_{slow}) decay times using the following equation:

$$I(t) = A_{fast}\exp(-\frac{t}{\tau_{fast}}) + A_{slow}\exp(-\frac{t}{\tau_{slow}}) \quad (1)$$

where I represents the PL intensity as a function of time(t), and A_{fast}, A_{slow} correspond to fast (non radiative) and slow (radiative) decay coefficients, respectively. The A and τ values of each sample are summarized in table 2. According to Iwata's model,[44] this bi-exponential behaviour is attributed to two different types of regions within the QD plane, *i.e.* regions with purely radiative channels and other ones with additional and competing non-radiative recombination centers. τ_{slow} defines the radiative lifetime, while τ_{fast} is a combination of both radiative and non-radiative lifetimes.[43] Decay times within a few tens of ns down to the sub-ns range have been measured (after deconvoluting from the width of the laser pulse) which are much shorter than typical times found for GaN QDs.[22,23] A main reason is that shorter τ_{fast} and τ_{slow} are observed when the QD heights get smaller, *i.e.* GaN QDs present heights around 4-5 nm compared to 1.5-2.6 nm in the case of the present $Al_yGa_{1-y}N$ QDs. This is confirmed in the case of samples A, C and D which have the highest average QD heights (*i.e.* ~ 2.5-2.6 nm) and

present the longest τ_{fast} and τ_{slow} values. On the contrary, samples E and G, for which the QDs show the smallest average heights (*i.e.* 1.5 nm) give the shortest lifetimes. In the cases of samples B and F, which present intermediate average QD heights (*i.e.* between 1.8-2.2 nm), decay time values contained between the two previous cases are found. It is known that the presence of an internal electric field in polar QD-based nitride heterostructures leads to a decrease of the electron and hole wavefunction overlap and a reduction of the oscillator strength with increasing QD heights, leading to longer PL intensity decay times.[40] In addition, a low level of surface recombination centers in the QDs would also lead to shorter τ_{fast} and τ_{slow} values, and could be due to the smaller available surface area of QDs presenting lower average QD heights.

From the exponential fits of the PL decay times (figure 6), A_{fast} and A_{slow} coefficients have been determined according to equation (1). It appears that the ratios of A_{fast} over A_{slow} tend to decrease for increasing QD emission energies (table 2), similarly to the behaviour already observed when going from GaN to $Al_{0.1}Ga_{0.9}N$ QDs.[22] From these parameters, the IQE at LT of the sample series have been calculated (table 2) according to the relation:[43]

$$IQE - LT = \frac{A_{fast}\tau_{fast} + A_{slow}\tau_{slow}}{\left(A_{fast} + A_{slow}\right)\tau_{slow}} \qquad (2)$$

IQE-LT values between 11% and 66% have been obtained. In the series of samples with $Al_{0.1}Ga_{0.9}N$ QDs, a larger IQE-LT is found for higher QDs and larger Δx-y (sample C). IQE-LT values are similar when going from $Al_{0.1}Ga_{0.9}N$ to $Al_{0.2}Ga_{0.8}N$ QDs with similar heights and maintaining a large Δx-y (0.5-0.6) (samples C and D, respectively). Such results indicate that a larger confining potential is more efficient than a stronger wave function overlap in $Al_yGa_{1-y}N$ QDs with y values of 0.1 or 0.2. However, it clearly appears that the largest IQE-LT values are obtained for QDs with larger Al composition y, *i.e.* for samples E to G, for which Δx-y is moderate (0.3-0.4).

2.3. PL radiative efficiency and IQE

From the PL and TRPL measurements, it is shown that the PL efficiency at RT and the IQE-LT are larger when Δx-y is increased in the case of QDs with lower y (10 - 20%) or when the QDs have larger y compositions (30 - 40%). By combining these results, the IQE of the different $Al_yGa_{1-y}N$ QD active regions at RT have been calculated. At this stage, it is important to note that the determination of an absolute value of IQE in QD-based nitride materials is very difficult and precautions should be taken. From the literature, it has been shown that the determination of the IQE in QWs by temperature dependent PL measurements depends on the excitation power density.[44,45] In our experiments, we have chosen an excitation power density of 470 W/cm^2. As for QWs, we found out the IQE is strongly dependent on the excitation power density even at LT, which indicates that non-radiative recombination processes are active. A similar behavior was reported in our group in the case of GaN QDs grown on $Al_{0.5}Ga_{0.5}N$.[46] In addition, the situation in the case of QDs is even more complex than for QWs due to the fluctuations in the QDs sizes (height and diameter) and compositions, as discussed in the case of $Al_{0.1}Ga_{0.9}N$ QDs grown on $Al_{0.5}Ga_{0.5}N$.[27] This is the reason why we have determined the IQE of the QDs at LT by performing TRPL measurements which are more adapted to the study of active regions made of QDs. Indeed, since we are dealing with samples presenting inhomogeneous distributions of defects and QDs at the scale of the laser spot, it appears that the situation is analogous of the situation in the samples described by Iwata et al.:[43] at LT, the laser spot shines two kinds of regions of the sample. In the first one, with a high densities of non radiative centers, the recombination dynamics are ruled by a typical decay time τ_{fast} while in the second one (of crystalline quality weakly affected or almost non-affected by such defects) the recombination dynamics are ruled by a decay time τ_{slow}. The resulting PL intensity decay is ruled by a two-component kinetics with proportions A_{fast} and its complementary A_{slow}. Iwata et al. suggested identifying τ_{slow} as the value of the radiative decay time (or to a close

representative of its value) while both radiative and non-radiative recombinations contribute to τ_{fast}. The interpretation of the value of τ_{fast} is then made within the context of a prey-predator description where the predators are the non-radiative recombination centers and the relative population of preys (radiatively recombining electron-hole pairs) and predators (electron-hole pairs trapped by non-radiative recombination centers) vary according to Lotka-Volterra coupled equations. This model is valid when clear and unambiguous fitting of the decay time is achievable, which is the case here and the values of IQEs framed by this determination match very well with the time-integrated PL features. Consequently, this model appears to be well adapted to our QD based active regions. However, the major drawback of the model is its limitation to the LT range so that cross talking between both regions is not active. Therefore, we cannot use it without including complementary interactions for the high temperature range and this is the reason why we have chosen to use the temperature dependent PL measurements as a complementary method to determine the IQE of the QDs at RT.

Given the approximations made and the complexity of the QD samples, the important point of the discussion here is the comparison of the IQE as a function of the QD designs and active region characteristics, *i.e.* the QD composition y and the QD height along with the Al composition difference between the QDs and the cladding layer (Δx-y). Therefore, in order to be able to compare the QD PL characteristics as much as possible, we have chosen to keep constant the PL excitation intensity at a moderate and constant continuous wave PL excitation power density to prevent as much as possible to be in potential situations where the IQE would be decreasing due to strong non radiative recombination processes or to an important saturation of states.[45] As a result, by calculating the product of the IQE-LT value determined by TRPL with the R_{PL} ratio between LT and RT measured by PL, we have estimated the IQE at RT of the complete sample series as reported in table 2, following the relation:

$$IQE = IQE\text{-}LT \times I_{PL}(RT) / I_{PL}(LT) \qquad (3)$$

Comparing the IQE values, it is then possible to put into evidence some specific trends on the design of QD active regions for UV emission, as highlighted in figure 7: in this figure, the IQE at RT has been plotted as a function of the QD PL energy at 300K and Δx-y. Importantly, the largest IQE (*i.e.* corresponding to the largest dots in the figure which sizes are proportional to the square root of the IQE value) are found for QDs emitting at shorter wavelengths, *i.e.* in the UVB and UVC ranges for which the EQE values of LEDs are strongly decreasing. IQE values between 5% and 20% are found, as indicated by a grey line in figure 7. Specifically, in the case of QDs emitting below 300 nm (*i.e.* between 4.18 and 4.49 eV), the IQE is reaching 10% at 297 nm and 19.8% at 276 nm. These values are obtained despite the very large dislocation densities (> 10^{10} cm^{-2}) in our structures, confirming the strong confinement of carriers, which increases their radiative recombination.

Our results also indicate that a larger confining potential is more efficient than a stronger wave function overlap (*i.e.* QDs with smaller heights) in $Al_yGa_{1-y}N$ QDs with y values of 0.1 or 0.2 (for samples A to D). However, it clearly appears that the largest IQE values are obtained for QDs with a larger Al composition y (for samples E to G). Obviously, in these cases, the radiative efficiency of the QDs does not obey the same rules than in the previous ones since they present smaller average heights and reduced chemical contrasts (Δx-y = 0.3-0.4). This behavior seems to indicate that the growth mechanisms of strained nanometer thick layers are influenced by the alloy Al composition, considering that the same growth conditions (growth rates, III / V ratio and temperature) have been used to fabricate the samples. Actually, it has been reported that thick $Al_xGa_{1-x}N$ layers grown by plasma assisted MBE present composition fluctuations for growth temperatures above 670°C,[47] and for Al composition of 50% or below.[48] Indeed, such growth temperatures and Al compositions correspond to the ones used for the fabrication of the $Al_yGa_{1-y}N$ QDs. Furthermore, these growth mechanisms are at the origin of

localization at the nanometer scale, *i.e.* at the scale of a QD, and therefore could modify the QD confining potential and associated carrier confinement, leading to an improvement of the IQE.

V. CONCLUSION

In summary, $Al_yGa_{1-y}N$ QDs with a nominal composition y varying from 10% to 40% have been grown by MBE in $Al_xGa_{1-x}N$ (0001) cladding layers with x equals to 0.5 or 0.7. Their morphological and optical properties have been investigated as a function of different growth parameters including the $Al_yGa_{1-y}N$ deposited amount, the QD Al composition y and Δx-y (*i.e.* the Al composition difference between the QDs and the cladding layer related to the band gap difference ΔE_g). It is observed that the average QD height is proportional to the deposited amount, and that high QD densities above 10^{11} cm^{-2} are obtained whatever the QD growth procedure details. Regarding the photoluminescence (PL) characteristics, it is shown that the integrated PL intensity temperature dependence is minimized in the case of a higher Δx-y (0.5 - 0.6) for low y values (0.1 – 0.2) and for QDs with high y values (0.3 – 0.4). In addition, time-resolved PL measurements (TRPL) performed at low temperature (LT) have evidenced a two-decay behaviour of the PL intensity, which is attributed to the presence of non-radiative recombination channels. Performing a fit of the different TRPL spectra, the IQE of the different QD designs have been determined at LT (8K) and show a strong variation from 11% to 66% among the samples. Importantly, larger IQE values have been obtained for QDs emitting at higher energies, *i.e.* in the UVB and UVC spectral regions. Combined with the PL intensity ratios determined between LT and RT (300K), IQE values between 5 and 20% at RT have been estimated for QDs emitting in the 276-308 nm range: as a trend, larger IQE values were found for QDs emitting at shorter wavelengths (*i.e.* QDs with a higher Al composition y), and for QDs capped in a cladding layer with a higher Al composition x in the case of QDs emitting at larger wavelengths (*i.e.* QDs with a lower Al composition y). In conclusion, this study shows the

potential of $Al_yGa_{1-y}N$ QDs as efficient UV emitters using a single step growth process and a basic heterostructure design with dislocation densities above 10^{10} cm^{-2}. Furthermore, the QD IQE was found to be higher in the deeper UV region, where improvements in the IQE of LEDs are mostly desirable.

ACKNOWLEDGMENTS

The authors would like to thank D. Lefebvre, A. Courville, S. Vézian and B. Poulet for their invaluable technical assistance, fruitful discussions and scientific help. The TITAN TEM experiments have been performed on the Minatec Nanocharacterisation platform at CEA-Grenoble thanks to the French METSA network. One of us, Maxim Korytov, thanks Dr Jean-Luc Rouvière for his kind help at the microscope during the experiments. This work was supported by ANR Project (ANR-14-CE26-0025) "NANOGANUV". We also acknowledge support from GANEX (ANR-11-LABX-0014). GANEX belongs to the publicly funded "Investissements d'Avenir" program managed by the French ANR agency.

[1] M. Kneissl, T.-Y. Seong, J. Han, and H. Amano, Nature Photonics **13**, 233 (2019).

[2] See http://www.mercuryconvention.org/

[3] J. Enslin, F. Mehnke, A. Mogilatenko, K. Bellmann, M. Guttmann, C. Kuhn, J. Rass, N. Lobo-Ploch, T. Wernicke, M. Weyers, and M. Kneissl, J. Crystal Growth **464**, 185 (2017).

[4] T. Takano, T. Mino, J. Sakai, N. Noguchi, K. Tsubaki, and H. Hirayama, Appl. Phys. Express **10**, 031002 (2017).

[5] M. Shatalov, W. Sun, R. Jain, A. Lunev, X. Hu, A. Dobrinsky, Y. Bilenko, J. Yang, G. A. Garrett, L. E. Rodak, M. Wraback, M. Shur, and R. Gaska, Semicond. Sci. Technol. **29** 084007 (2014).

[6] Y. Kashima, N. Maeda, E. Matsuura, M. Jo, T. Iwai, T. Morita, M. Kokubo, T. Tashiro, R. Kamimura, Y. Osada, H. Takagi, and H. Hirayama, Appl. Phys. Express **11**, 012101 (2018).

[7] N. Susilo, S. Hagedorn, D. Jaeger, H. Miyake, U. Zeimer, C. Reich, B. Neuschulz, L. Sulmoni, M. Guttmann, F. Mehnke, C. Kuhn, T. Wernicke, M. Weyers, and M. Kneiss, Appl. Phys. Lett. **112**, 041110 (2018).

[8] T.-Y. Wang, C.-T. Tasi, C.-F. Lin, and D.-S. Wuu, Sci. Rep. **7**, 14422 (2017).

[9] M. A. Khan, N. Maeda, M. Jo, Y. Akamatsu, R. Tanabe, Y. Yamada, and H. Hirayama, J. Mater. Chem. C **7**, 143 (2019).

[10] A. Knauer, T. Kolbe, J. Rass, H. K. Cho, C. Netzel, S. Hagedorn, N. Lobo-Ploch, J. Ruschel, J. Glaab, S. Einfeldt, and M. Weyers, Jpn. J. Appl. Phys. **58**, SCCC02 (2019).

[11] M. H. Crawford, Semiconductors and Semimetals **96**, 3 (2017).

[12] K. Ban, J.-i. Yamamoto, K. Takeda, K. Ide, M. Iwaya, T. Takeuchi, S. Kamiyama, I. Akasaki, and H. Amano, Appl. Phys. Express **4**, 052101 (2011).

[13] T. Kohno, Y. Sudo, M. Yamauchi, K. Mitsui, H. Kudo, H. Okagawa, and Y. Yamada, Jpn. J. Appl. Phys. **51** 072102 (2012).

[14] J. Sellés, C. Brimont, G. Cassabois, P. Valvin, T. Guillet, I. Roland, Y. Zeng, X. Checoury, P. Boucaud, M. Mexis, F. Semond, and B. Gayral, Sci. Rep. **6**, 21650 (2016).

[15] X. Rong, X. Wang, S. V. Ivanov, X. Jiang, G. Chen, P. Wang, W. Wang, C. He, T. Wang, T. Schulz, M. Albrecht, V. Jmerik, A. Toropov, V. Ratnikov, V. Kozlovsky, V. Martovitsky, P. Jin, F. Xu, X. Yang, Z. Qin, W. Ge, J. Shi, and B. Shen, Adv. Mater. **28**, 7978 (2016).

[16] S. M. Islam, V. Protasenko, K. Lee, S. Rouvimov, J. Verma, H. Xing, and D. Jena, Appl. Phys. Lett. **111**, 091104 (2017).

[17] A. Bhattacharyya, T. D. Moustakas, L. Zhou, D. J. Smith, and W. Hug, Appl. Phys. Lett. **94**, 181907 (2009).

[18] M. Kaneda, C. Pernot, Y. Nagasawa, A. Hirano, M. Ippommatsu, Y. Honda, H. Amano, and I. Akasaki, Jpn. J. Appl. Phys. **56**, 061002 (2017).

[19] Y. Liao, C. Thomidis, C. Kao, and T. D. Moustakas, Appl. Phys. Lett. **98**, 081110 (2011).

[20] J Brault, B. Damilano, A. Kahouli, S. Chenot, M. Leroux, B. Vinter and J. Massies, J. Crystal Growth **363**, 282 (2013).

[21] C. Himwas, M. den Hertog, E. Bellet-Amalric, R. Songmuang, F. Donatini, Le Si Dang, and E. Monroy, J. Appl. Phys. **116**, 023502 (2014).

[22] J. Brault, S. Matta, T. H. Ngo, M. Korytov, D. Rosales, B. Damilano, M. Leroux, P. Vennéguès, M. Al Khalfioui, A. Courville, O. Tottereau, J. Massies, and B. Gil, Jpn. J. Appl. Phys. **55**, 05FG06 (2016).

[23] S. Matta, J. Brault, T. H. Ngo, B. Damilano, M. Korytov, P. Vennéguès, M. Nemoz, J. Massies, M. Leroux, and B. Gil, J. Appl. Phys. **122**, 085706 (2017).

[24] Y. Liao, C.-k. Kao, C. Thomidis, A. Moldawer, J. Woodward, D. Bhattarai, and T. D. Moustakas, Phys. Status Solidi C **9**, 798 (2012).

[25] C. Himwas, R. Songmuang, Le Si Dang, J. Bleuse, L. Rapenne, E. Sarigiannidou, and E. Monroy, Applied Physics Letters **101**, 241914 (2012).

[26] S. Contreras, L. Konczewicz, J. Ben Messaoud, H. Peyre, M. Al Khalfioui, S. Matta, M. Leroux,B. Damilano, J. Brault, Superlattices and Microstructures **98**, 253 (2016).

[27] S. Matta, J. Brault, T. H. Ngo, B. Damilano, M. Leroux, J. Massies, and B. Gil, Superlattices & Microstructures **114**, 161 (2018).

[28] J. Verma, P. K. Kandaswamy, V. Protasenko, A. Verma, H. G. Xing, and D. Jena, Appl. Phys. Lett. **102**, 041103 (2013).

[29] J. Brault, S. Matta, T. H. Ngo, D. Rosales, M. Leroux, B. Damilano, M. Al Khalfioui, F. Tendille, S. Chenot, P. De Mierry, J. Massies, and B. Gil, Mater. Sci. Semicond. Process. **55**, 95 (2016).

[30] J. Brault, D. Rosales, B. Damilano, M. Leroux, A. Courville, M. Korytov, S. Chenot, P. Vennéguès, B. Vinter, P. De Mierry, A. Kahouli, J. Massies, T. Bretagnon, and B. Gil, Semicond. Sci. Technol. **29**, 084001 (2014).

[31] J. Brault, M. Al Khalfioui, S. Matta, B. Damilano, M. Leroux, S. Chenot, M. Korytov, J. E. Nkeck, P. Vennéguès, J. –Y. Duboz, J. Massies, and B. Gil, Semicond. Sci. Technol. **33**, 075007 (2018).

[32] B. Damilano, N. Grandjean, F. Semond, J. Massies, and M. Leroux, Appl. Phys. Lett. **75**, 962 (1999).

[33] N. Grandjean, and J. Massies, Appl. Phys. Lett. **71**, 1816 (1997).

[34] T. Huault, J. Brault, F. Natali, B. Damilano, D. Lefebvre, L. Nguyen, M. Leroux, and J. Massies, Appl. Phys. Lett. **92**, 051911 (2008).

[35] M. Nemoz, R. Dagher, S. Matta, A. Michon, P. Vennéguès, and J. Brault, J. Cryst. Growth **461**, 10 (2017).

[36] B. Daudin, F. Widmann, G. Feuillet, Y. Samson, M. Arlery, and J. L. Rouvière, Phys. Rev. B **56**, R7069 (1997).

[37] J. Tersoff, and F. K. LeGoues, Phys. Rev. Lett. **72**, 3570 (1994).

[38] B. Damilano, J. Brault, and J. Massies, J. Appl. Phys. **118**, 024304 (2015).

[39] M. Korytov, M. Benaissa, J. Brault, T. Huault, T. Neisius, P. Vennégues, Appl. Phys. Lett. **94**, 143105 (2009).

[40] T. Bretagnon, P. Lefebvre, P. Valvin, R. Bardoux, T. Guillet, T. Taliercio, B. Gil, N. Grandjean, F. Semond, B. Damilano, A. Dussaigne, and J. Massies, Phys. Rev. B **73**, 113304 (2006).

[41] M. Leroux, S. Dalmasso, F. Natali, S. Helin, C. Touzi, S. Laügt, M. Passerel, F. Omnès, F. Semond, J. Massies,and P. Gibart, phys. stat. sol. (b) **234**, 887 (2002).

[42] J.L. Rouvière, J. Simon, N. Pelekanos, B. Daudin, and G. Feuillet Appl. Phys. Lett. **75**, 2632 (1999).

[43] Y. Iwata, R. G. Banal, S. Ichikawa, M. Funato, and Y. Kawakami, J. Appl. Phys. **117**, 075701 (2015).

[44] S. Watanabe, N. Yamada, M. Nagashima, Y. Ueki, C. Sasaki, Y. Yamada, T. Taguchi, K. Tadatomo, H. Okagawa, and H. Kudo, Appl. Phys. Lett. **83**, 4906 (2003).

[45] Y. Yamada, K. Iwamura, T. Kuronaka, N. Shinomura, T. Taguchi, H. Kudo, and H. Okagawa, J. Light & Vis. Env. **32**, 191 (2008).

[46] M. Leroux, J. Brault, A. Kahouli, D. Elmaghraoui, B. Damilano, P. de Mierry, M. Korytov, J.-H. Kim, Y.-H. Cho, J. Appl. Phys. **116**, 034308 (2014).

[47] V. Fellmann, P. Jaffrennou, D. Sam-Giao, B. Gayral, K. Lorenz, E. Alves, and B. Daudin, Jpn. J. Appl. Phys. **50**, 031001 (2011).

[48] M. Gao, S. T. Bradley, Y. Cao, D. Jena, Y. Lin, S. A. Ringel, J. Hwang, W. J. Schaff, and L. J. Brillson, J. Appl. Phys. **100**, 103512 (2006).

[50] N. Nepal, J. Li, M. L. Nakarmi, J. Y. Lin, and H. X. Jiang, Appl. Phys. Lett. **87**, 242104 (2005).

Figure captions:

FIG. 1. Schematics of the QD sample structure including the initial growth of a 30 nm-thick GaN buffer layer on sapphire, followed by the growth of a 100-150 nm-thick AlN layer and a 800-1000 nm-thick $Al_xGa_{1-x}N$ cladding layer. The active region is made of an $Al_yGa_{1-y}N$ QD plane (capped by a 30 nm-thick $Al_xGa_{1-x}N$ layer) and a final $Al_yGa_{1-y}N$ QD plane at the surface. Depending on the sample, the Al concentration x is equal to 0.5 or 0.7 and to 0.1, 0.2, 0.3 or 0.4 for the Al QD composition y.

FIG. 2. Atomic force microscopy images (500x500 nm^2) of $Al_yGa_{1-y}N$ QDs for the complete sample series from (a) sample A to (g) sample G.

FIG. 3. High-angle annular dark-field imaging in scanning transmission electron microscopy mode images of $Al_yGa_{1-y}N$ QDs grown in an $Al_{0.7}Ga_{0.3}N$ (0001) cladding layer for an Al composition y equals to: a) 0.1 (sample C), b) 0.2 (sample D), c) 0.3 (sample E) and d) 0.4 (sample F).

FIG. 4. Normalized photoluminescence spectra measured at RT of $Al_yGa_{1-y}N$ QDs for the whole sample series.

FIG. 5. Photoluminescence spectra measured at LT (thin lines) and RT (bold lines) of the $Al_yGa_{1-y}N$ QD sample series for (a) samples A to D and (b) samples E to G.

FIG. 6. Time-resolved photoluminescence spectra (diamonds) recorded at LT of the $Al_yGa_{1-y}N$ QDs sample series for (a) samples A to D and (b) samples E to G. The bold lines in the figures are fits using equation (1).

FIG. 7. (a) Internal quantum efficiency at RT (IQE) of the QD sample series (from A to G) as a function of the photoluminescence energy and the Al composition difference between the QDs and the cladding layer (Δx-y). The size of each dot is proportional to the square root of the IQE of each QD sample. The vertical and horizontal lines are connecting the dots to the values referring to the PL energy and Δx-y associated to each sample. The grey line is a guide for the eyes. (b) Variation of the PL emission energy as a function of QD height and the composition difference Δx-y.

Table 1. Description of the QD sample series: aluminum composition in the $Al_xGa_{1-x}N$ cladding layer and $Al_yGa_{1-y}N$ QDs, deposited amount of $Al_yGa_{1-y}N$, structural properties of the QDs (average dimensions and densities determined by combining AFM and TEM measurements) and photoluminescence emission energy and corresponding wavelength measured at room temperature (RT).

Sample	$Al_xGa_{1-x}N$ cladding layer Al composition	$Al_yGa_{1-y}N$ QDs		QD structural properties			Photoluminescence	
		Composition y	Deposited amount (monolayers)	QD height (nm)	QD diameter (nm)	QD density (cm^{-2})	Energy (eV)	Wavelength (nm)
A	0.5	0.1	10	2.5 ± 0.5	10 ± 5	$5.0(\pm 1)x10^{11}$	3.73	332
B	0.5	0.1	7	1.8 ± 0.5	8 ± 4	$1.5(\pm 1)x10^{11}$	3.95	314
C	0.7	0.1	10	2.6 ± 0.3	10 ± 3	$2.4(\pm 1)x10^{11}$	3.73	332
D	0.7	0.2	10	2.6 ± 0.3	10 ± 3	$5.4(\pm 1)x10^{11}$	4.02	308
E	0.7	0.3	6	1.5 ± 0.3	8 ± 4	$2.2(\pm 1)x10^{11}$	4.18	297
F	0.7	0.4	8	2.2 ± 0.4	10 ± 4	$2.6(\pm 1)x10^{11}$	4.12	301
G	0.7	0.4	6	1.5 ± 0.4	8 ± 4	$4.8(\pm 1)x10^{11}$	4.49	276

Table 2. Summary of the main optical characteristics of the $Al_yGa_{1-y}N$ QD sample series determined by PL and TRPL: the PL spectrally integrated intensity ratio (R_{PL}) between LT and RT, the slow (τ_{slow}) and fast (τ_{fast}) decay times and A_{fast} and A_{slow} coefficients deduced from the TRPL decay times, the low temperature (LT) internal quantum efficiency (IQE_{LT}) deduced from ref. 44 and the IQE of the QDs determined by the product of IQE_{LT} by R_{PL}. The theoretical band gap energy difference between the QD and the cladding layer (ΔE_g) given in the table has been determined from ref. 50.

Samples	Active region design		$R_{PL} = I_{RT}/I_{LT}$ (%)	τ_{fast} (ns)	τ_{slow} (ns)	A_{fast}	A_{slow}	IQE_{LT} (%)	IQE (%)
	QD/cladding layer	ΔE_g							
A	$Al_{0.1}Ga_{0.9}N/Al_{0.5}Ga_{0.5}N$	0.87 eV	10 ± 1	2.2	18.3	929.6	60.6	17	1.7
B	$Al_{0.1}Ga_{0.9}N/Al_{0.5}Ga_{0.5}N$	0.87 eV	10 ± 1	1.1	14.4	1393.6	63.0	11	1.1
C	$Al_{0.1}Ga_{0.9}N/Al_{0.7}Ga_{0.3}N$	1.43 eV	15 ± 1	3.7	18.6	1943.4	275.3	30	4.5
D	$Al_{0.2}Ga_{0.8}N/Al_{0.7}Ga_{0.3}N$	1.24 eV	30 ± 2	2.1	16.8	972.9	182.9	26	7.8
E	$Al_{0.3}Ga_{0.7}N/Al_{0.7}Ga_{0.3}N$	1.03 eV	20 ± 2	0.87	2.3	487.6	111.7	50	10
F	$Al_{0.4}Ga_{0.6}N/Al_{0.7}Ga_{0.3}N$	0.80 eV	10 ± 1	0.82	4.0	346.7	228.7	52	5.2
G	$Al_{0.4}Ga_{0.6}N/Al_{0.7}Ga_{0.3}N$	0.80 eV	30 ± 2	0.11	0.60	76.9	55.2	66	19.8

FIG. 1.

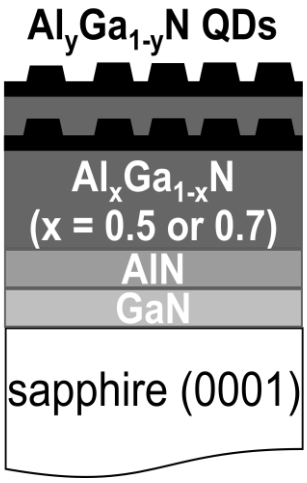

FIG. 2.

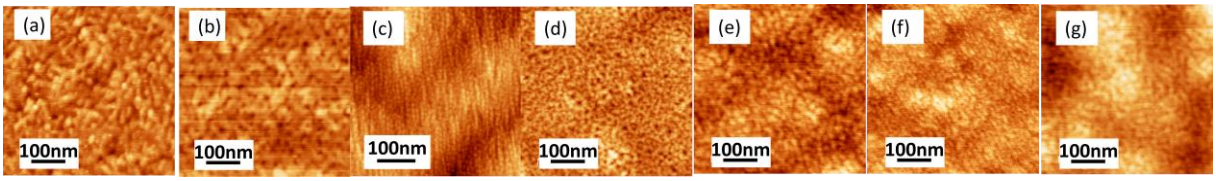

FIG. 3.

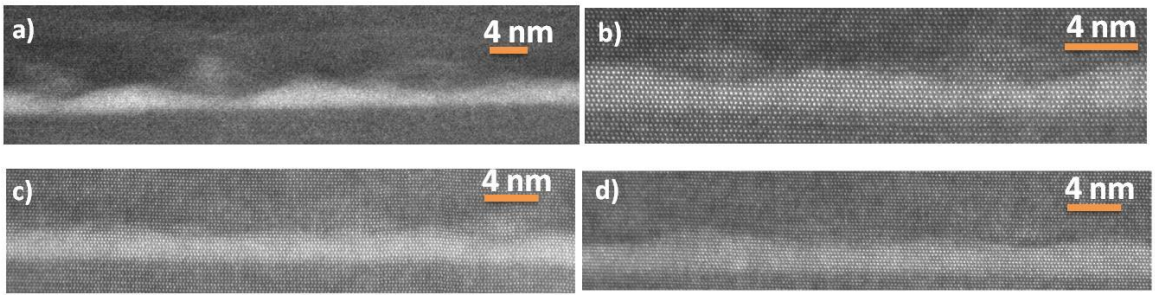

FIG. 4.

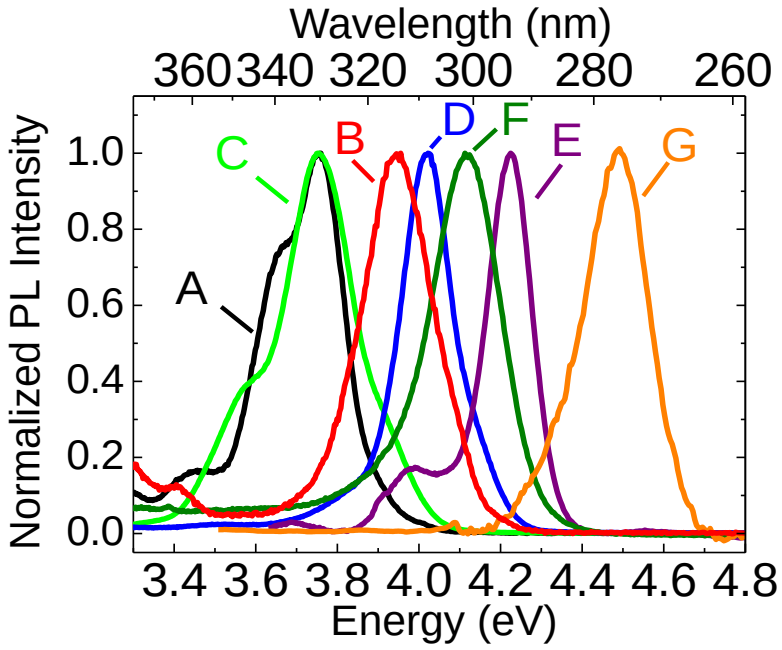
Wavelength (nm)
360 340 320 300 280 260
Normalized PL Intensity
1.0
0.8
0.6
0.4
0.2
0.0
A
C
B
D
F
E
G
3.4 3.6 3.8 4.0 4.2 4.4 4.6 4.8
Energy (eV)

FIG. 5.

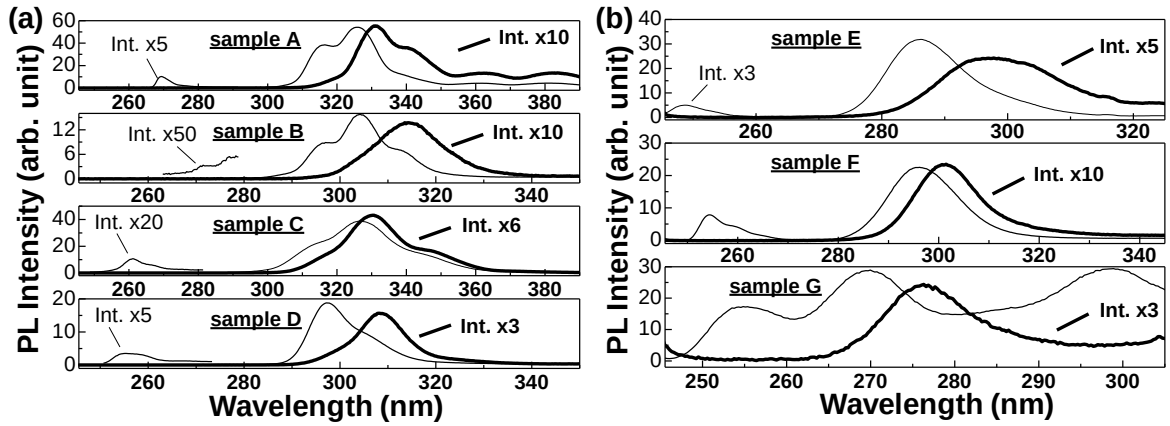
(a)
sample A
Int. x5
Int. x10
sample B
Int. x50
Int. x10
sample C
Int. x20
Int. x6
sample D
Int. x5
Int. x3
PL Intensity (arb. unit)
Wavelength (nm)
(b)
sample E
Int. x3
Int. x5
sample F
Int. x10
sample G
Int. x3
PL Intensity (arb. unit)
Wavelength (nm)

FIG. 6.

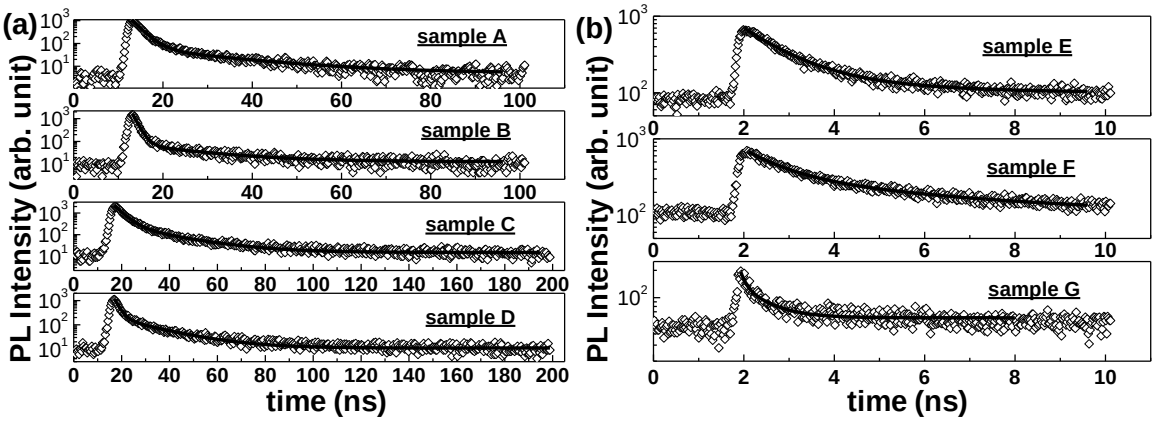
(a)
(b)
sample A
sample B
sample C
sample D
sample E
sample F
sample G
PL Intensity (arb. unit)
time (ns)

FIG. 7.

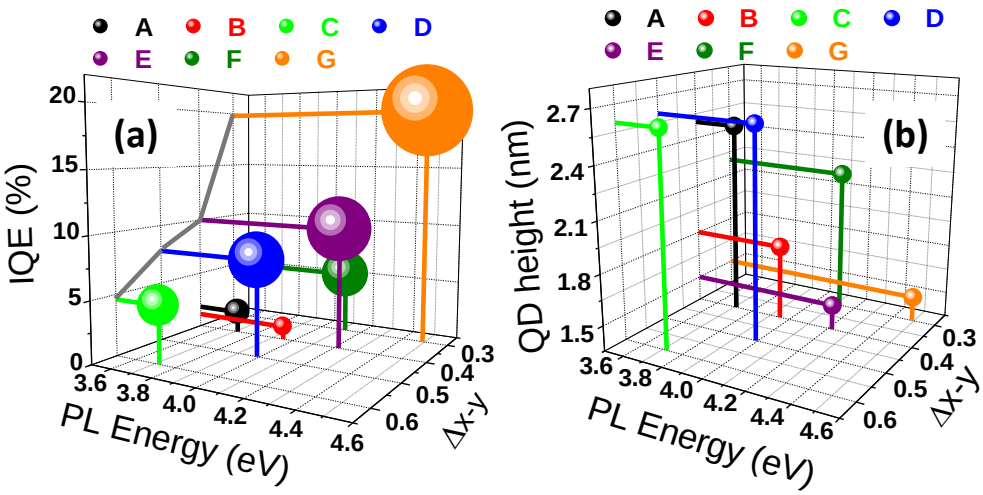
A
B
C
D
E
F
G
(a)
IQE (%)
20
15
10
5
0
3.6
3.8
4.0
4.2
4.4
4.6
PL Energy (eV)
0.3
0.4
0.5
0.6
Δx-y
(b)
QD height (nm)
2.7
2.4
2.1
1.8
1.5

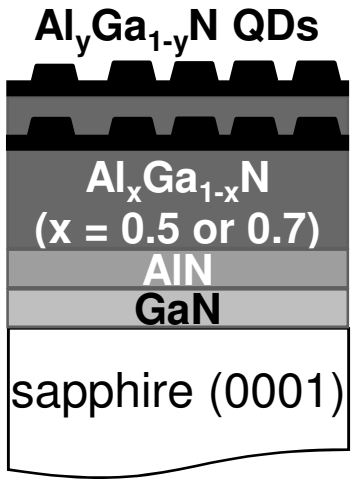
$Al_yGa_{1-y}N$ QDs
$Al_xGa_{1-x}N$
(x = 0.5 or 0.7)
AlN
GaN
sapphire (0001)

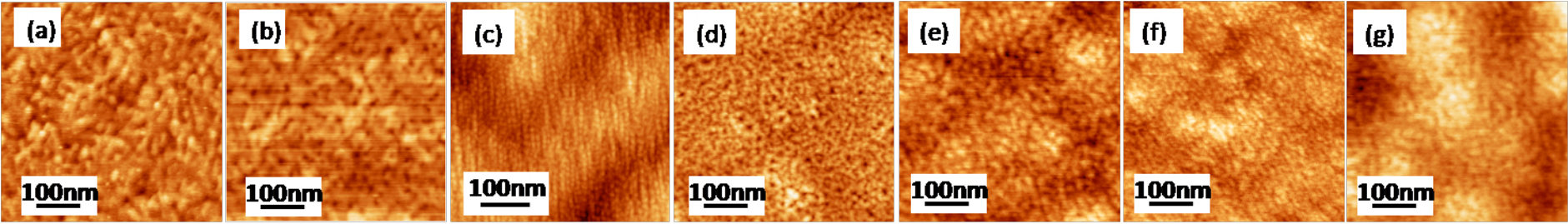
(a)
100nm
(b)
100nm
(c)
100nm
(d)
100nm
(e)
100nm
(f)
100nm
(g)
100nm

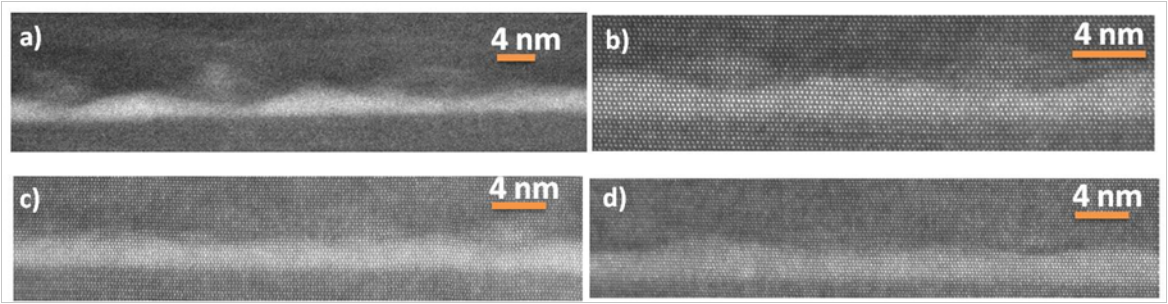
a)
4 nm
b)
4 nm
c)
4 nm
d)
4 nm

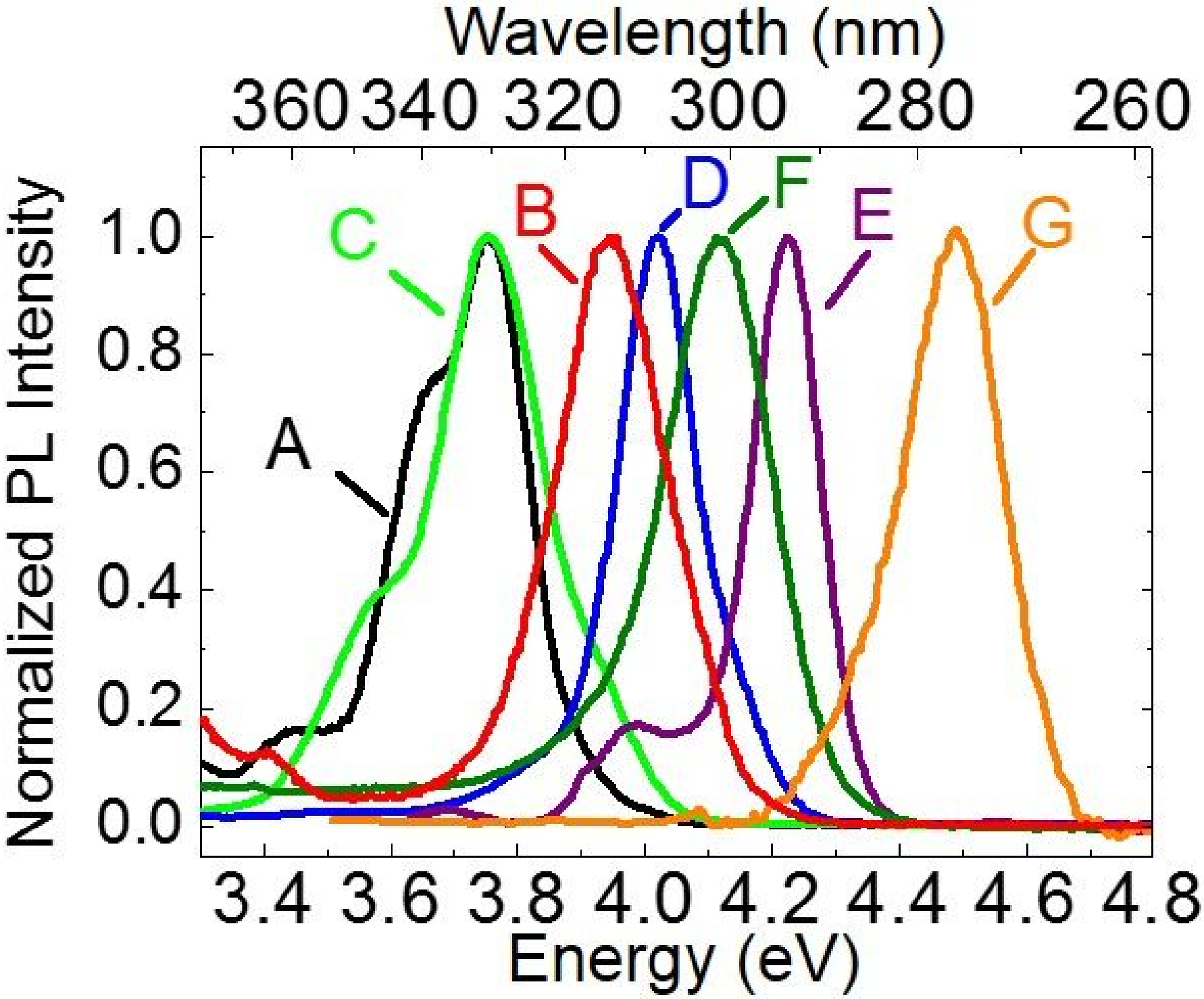
Wavelength (nm)
360 340 320 300 280 260
Normalized PL Intensity
1.0
0.8
0.6
0.4
0.2
0.0
A
C
B
D
F
E
G
3.4 3.6 3.8 4.0 4.2 4.4 4.6 4.8
Energy (eV)

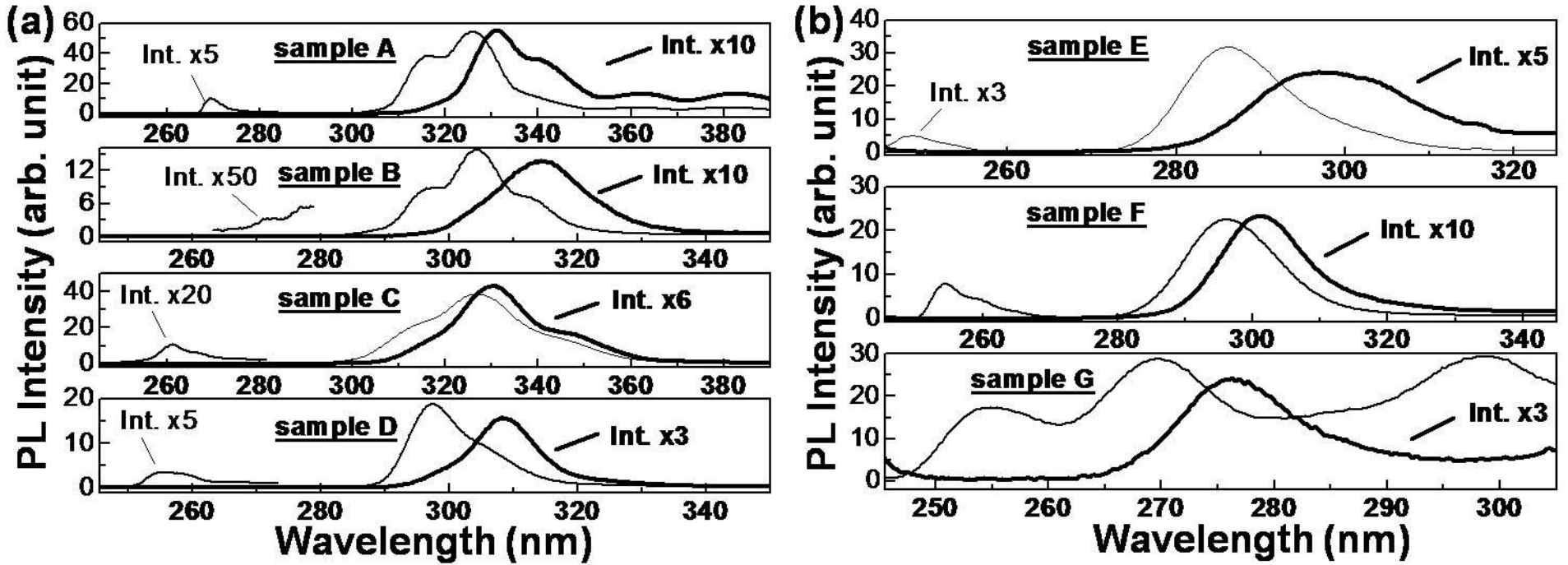
(a)
PL Intensity (arb. unit)
Int. x5
sample A
Int. x10
Int. x50
sample B
Int. x10
Int. x20
sample C
Int. x6
Int. x5
sample D
Int. x3
Wavelength (nm)
(b)
PL Intensity (arb. unit)
sample E
Int. x3
Int. x5
sample F
Int. x10
sample G
Int. x3
Wavelength (nm)

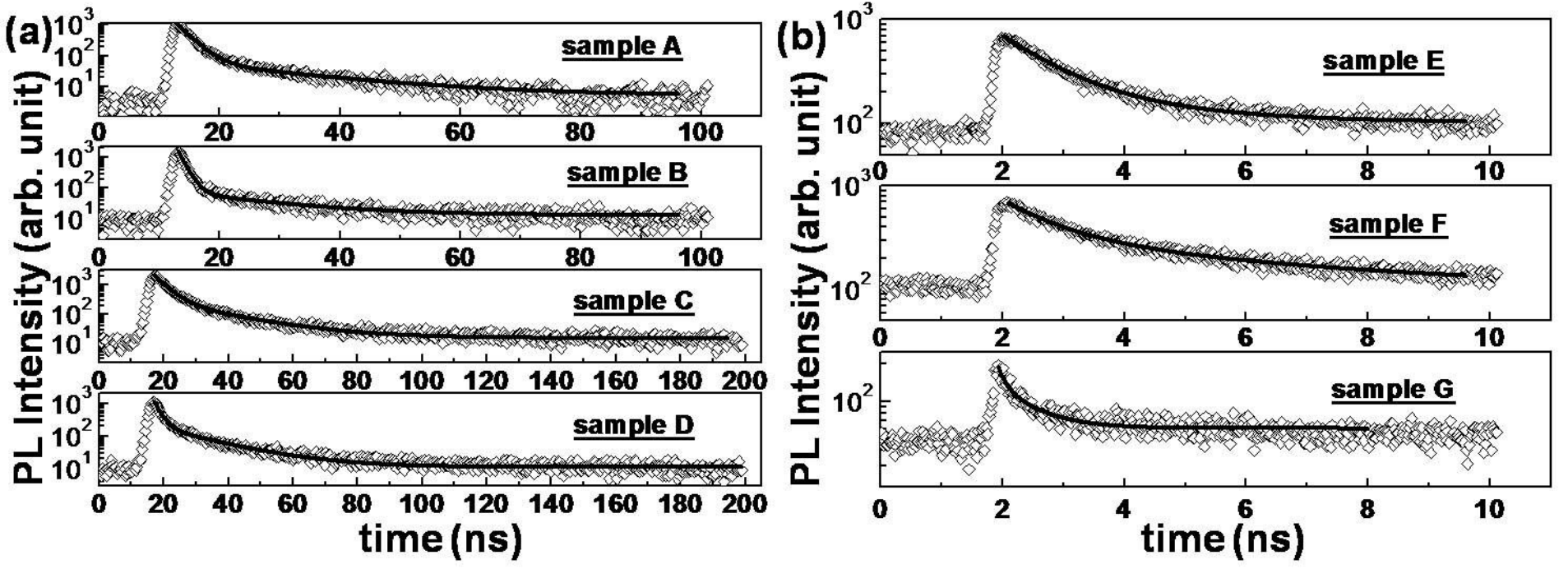
(a)
(b)
PL Intensity (arb. unit)
time (ns)
sample A
sample B
sample C
sample D
sample E
sample F
sample G

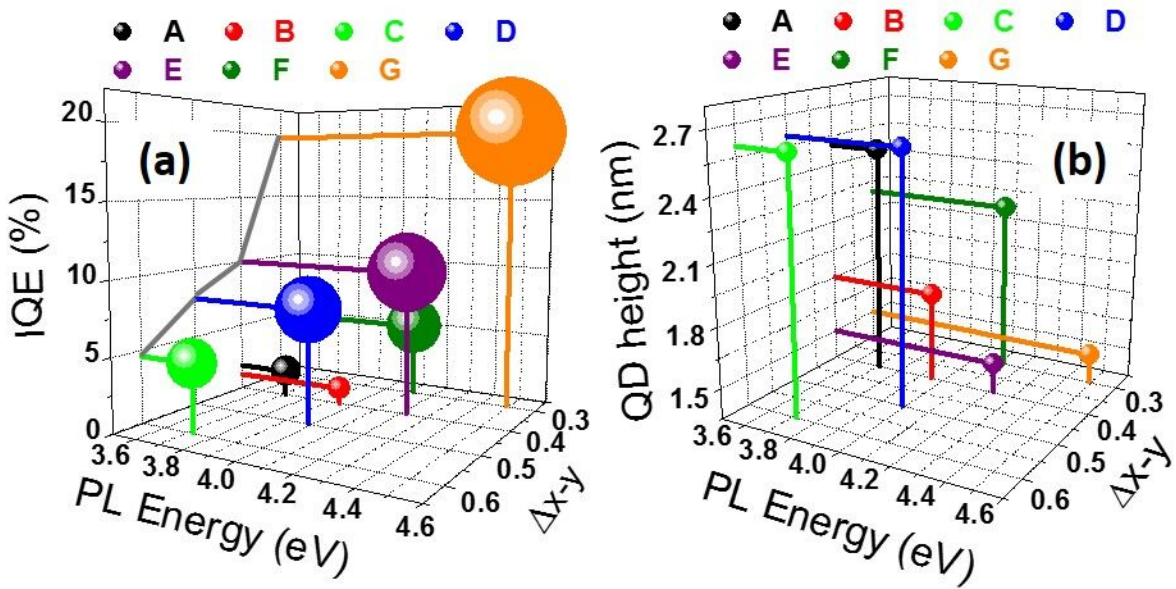
A
B
C
D
E
F
G
(a)
IQE (%)
20
15
10
5
0
3.6
3.8
4.0
4.2
4.4
4.6
PL Energy (eV)
0.3
0.4
0.5
0.6
Δx-y
(b)
QD height (nm)
2.7
2.4
2.1
1.8
1.5
3.6
3.8
4.0
4.2
4.4
4.6
PL Energy (eV)
0.3
0.4
0.5
0.6
Δx-y